High-Q Active Microwave Sensor Based on Microstrip Complementary Split-Ring Resonator (MCSRR) Structure for Dielectric Characterization

Hong-Yi Gan, Wen-Sheng Zhao, Da-Wei Wang, Jing Wang, Qi Liu, and Gaofeng Wang

MOE Engineering Research Center of Smart Micro-sensors and Micro-systems
School of Electronics and Information, Hangzhou Dianzi University, Hangzhou, 310018, China
honyigan@163.com, {wshzhao, davidw.zoeq, wangjing, liuqi67, gaofeng}@hdu.edu.cn

Abstract — This paper presents an active microwave sensor for the characterization of dielectric materials. The sensor is consisted of a microstrip complementary split-ring resonator (MCSRR) structure and an active feedback loop. The loop uses an amplifier to generate negative resistance to compensate the resonator's loss and increase the loaded quality factor. The developed sensor possesses the advantages of high quality factor, ultra-small electrical size, and high sensitivity. A prototype of the sensor is fabricated and measured for validation.

Index Terms — Active feedback loop, Microstrip Complementary Split-Ring Resonator (MCSRR), quality factor, sensor.

I. INTRODUCTION

Accurate measurement of complex permittivity of dielectric materials plays a vital role in healthcare, food safety, and industrial manufacturing [1]-[6]. To this end, microwave resonance planar sensors have been widely explored in recent years due to their low cost and easy fabrication [7]-[10]. In microwave resonance sensors, the resonant frequency and quality factor are related to the relative permittivity and electrical loss of the material under test. This is, as the MUT sample is loaded, the resonant frequency would shift downwards due to the increased resonator capacitance, while the quality factor is degraded due to the dielectric loss.

According to the frequency response characteristics, the microwave resonance planar sensors can be divided into two types, i.e., band-pass response and band-stop response. In [7] and [8], the split-ring resonator (SRR) and complementary split-ring resonator (CSRR) coupled microstrip transmission lines were used in the sensor design, and the complex permittivity of the MUT were extracted through the transmission zero. These two sensors act as band-stop filters. On the contrary, the microstrip SRR and microstrip CSRR (MCSRR) structures developed in [9] and [10] behave like band-pass filters, i.e., the transmission is close to 1 at the resonant point. It is evident that the band-pass sensor is more suitable than the band-stop sensor to characterize the dielectric loss. This is because that the dielectric loss is usually retrieved by the variation in the notch depth, which is difficult to discern in a band-stop resonator, thereby putting pressure on the design of peripheral circuit.

However, due to conductor loss and radiation, the resonant magnitude of band-pass sensor in the measurement is usually much smaller than theoretical value (i.e., 0 dB). To improve sensor resolution, it is necessary to increase the quality factor as much as possible. The active feedback loop with a microwave amplifier can generate negative resistance to compensate the resonator's loss, and therefore was utilized to enhance the sensor's quality factor [11], [12]. In this paper, an MCSRR-based sensor is presented for dielectric characterization. The active feedback loop is employed to improve the sensor resolution. The rest of this paper is organized as follows. Section II introduces the structure of the proposed active MCSRR-based sensor, with the operating principle discussed. Section III presents the experimental validation, and some conclusions are finally drawn in Section IV.

II. MCSRR-LOADED PLANAR SENSOR

Figure 1 shows the schematic of the proposed microwave resonance sensor, which is composed of an MCSRR and an active feedback loop. The MCSRR can be viewed as a band-pass resonator, where the transmitted energy reaches maximum at the resonant point. The active loop is formed by connecting two 1.5 mm wide L-shaped microstrip lines through the transistor, which is placed with 3.25 mm distance away from the feedline of MCSRR. The transistor is MRF947, which is a low-noise, high-gain amplifier with a unity-gain current frequency of 10 GHz. The bending points of two L-shaped microstrip lines are connected to VB and VC, respectively, through a 2.2 nH inductor to bring the DC bias voltage to the base and collector of the transistor at resonance (1.64 GHz). The electrode and the emitter of the transistor are grounded.

Submitted On: December 9, 2020
Accepted On: February 23, 2021

https://doi.org/10.47037/2021.ACES.J.360715

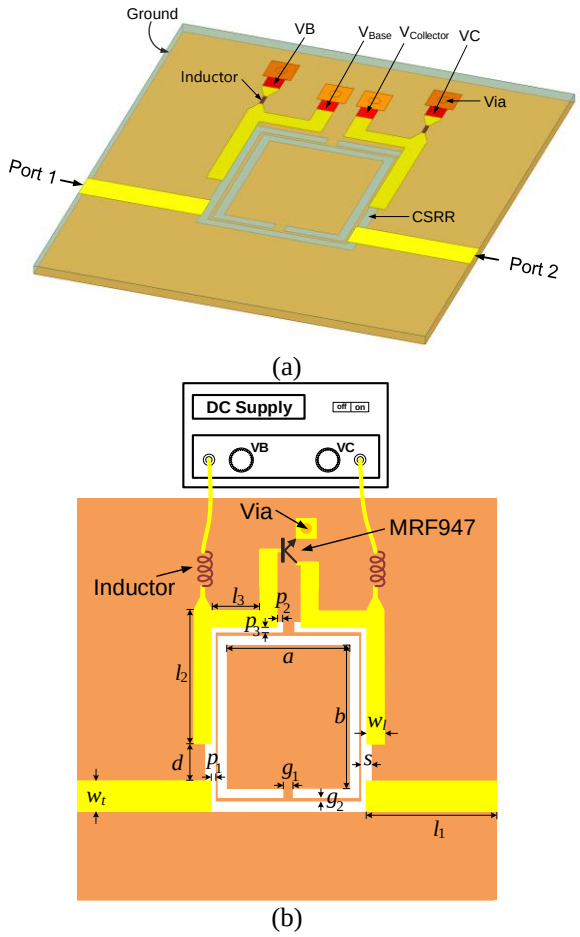

Fig. 1. (a) 3-D view and (b) planar view of the proposed MCSRR-based sensor.

The substrate is adopted as Rogers RO5880 with dielectric constant of 2.2 and loss tangent of 0.0009. The substrate dimension is 40mm×35mm×0.79mm. As shown in Fig. 1 (b), the width of the microstip line port is 2.5 mm, which is exactly matched to 50 Ω characteristic impedance. Detailed geometrical parameters are listed in Table 1. The MCSRR substrate occurs resonance when the resonant cavity stores an oscillating and balanced electric and magnetic energy. The resonant frequency changes when the distribution of the electromagnetic fields within the resonator perturbs. The change in the resonant frequency can be related to the MUT properties according to cavity perturbation theory:

$$\frac{\Delta f_r}{f_r} = \frac{\int_V (\Delta\varepsilon |E_0|^2 + \Delta\mu |H_0|^2) dV}{\int_V (\varepsilon_0 |E_0|^2 + \mu_0 |H_0|^2) dV}, \quad (1)$$

where Δf_r denotes the shift in the resonant frequency f_r, $\Delta\varepsilon$ and $\Delta\mu$ are the variations in the permittivity and permeability, ε_0 and μ_0 are the permittivity and permeability in vacuum, E_0 and H_0 are the electric and magnetic fields, and v denotes the perturbed volume.

Table 1: Geometrical parameters (Unit: mm)

Parameter	Value	Parameter	Value
w_t	2.5	l_1	11
l_2	11.25	l_3	4
a	10.2	b	12.2
s	0.8	g_1	1
g_2	0.3	p_1	0.5
p_2	0.38	p_3	0.22
w_l	1.5	d	3.25

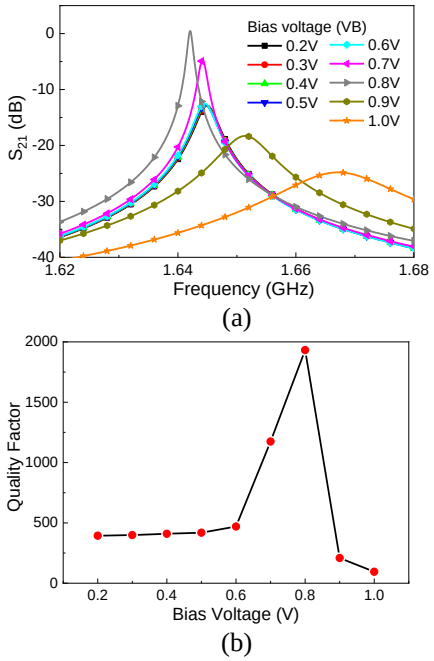

Fig. 2. (a) Transmission coefficient of the sensor with different bias voltages. (b) Quality factor versus bias voltage.

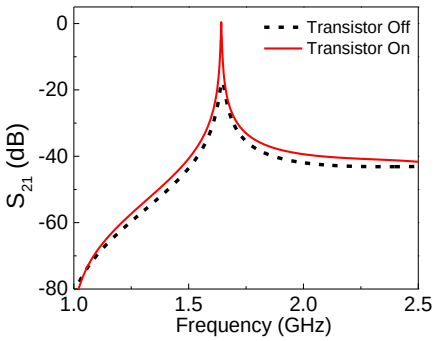

Fig. 3. Transmission coefficient of the sensor with different states of active loop. The bias voltage in the on state is 0.8 V.

To investigate the influence of active loop on the sensor quality factor, the frequency responses of the

designed sensor with active loop powered ON and OFF are captured and compared. Firstly, the sensor response of the original passive MCSRR-based sensor is simulated using commercial software ANSYS HFSS. HFSS is based on finite element method (FEM) that utilizes solutions of Maxwell's equations to compute the scattering parameters of each port. Then, the simulated scattering parameter matrix is input into the circuit simulator ADS. Since the physical parameters of the MCSRR structure, active loop, and lumped devices have been fixed, the only variable parameter is the gain controlled by the external voltage source (see Fig. 1 (b)). As shown in Fig. 2 (a), by tuning the bias voltage, the amplifier gain would be changed, thereby affecting the frequency response significantly. Here, the sensor quality factor is defined as the ratio of resonant frequency and 3 dB bandwidth, i.e., $Q = f_r/f_{3\mathrm{dB}}$. It is calculated that the quality factor of passive MCSRR-based sensor is about 92.8. With the bias voltage increasing to 0.5V, the sensor response is almost unchanged, while the quality factor is slightly increased from 393.7 to 469.9. As the bias voltage exceeds 0.6 V, the transistor enters linear operating region and generates high gain, which greatly increases the sensor quality factor. It can be seen in Fig. 2 (b) that the quality factor reaches maximum value of 1931.9 as the bias voltage equals 0.8 V. Fig. 3 shows the simulated sensor responses with ON-state and OFF-state active loop (the bias voltage in the ON-state is 0.8 V). As transistor is turned on, the resonant frequency is reduced from 1. 646 GHz to 1.642 GHz, implying the active loop has little influence on the resonant point and the measurement.

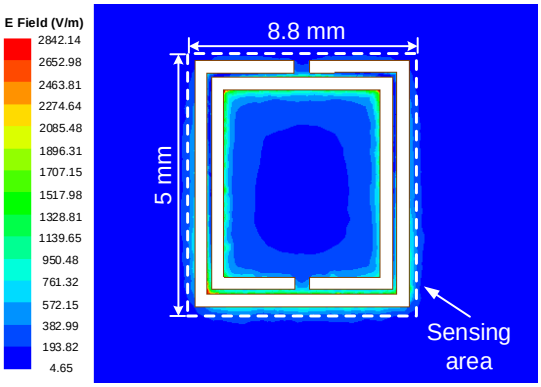

Fig. 4. Distribution of the electric field magnitude on the ground plane at the resonant frequency. The white dotted box in the middle represents the sensing area.

Further, the distribution of the electric field magnitude on the ground plane of the sensor is shown in Fig. 4. It is evident that the electric field intensity is mainly confined to the CSRR ring. The CSRR region, which is marked by the white dotted box in Fig. 4, is suitable to be used as sensing area to retrieve the complex permittivity of the MUT sample. To validate the sensor function, an 8.5 mm×5 mm×1 mm-size MUT sample is placed onto the sensing area of the proposed sensor. The sensor responses to the MUT sample with different complex permittivity are shown in Fig. 5. In the simulation, the relative permittivity ε_r' and loss tangent $\tan\delta_e$ of the MUT sample are varied from 1 to 10 and from 0 to 0.1, respectively.

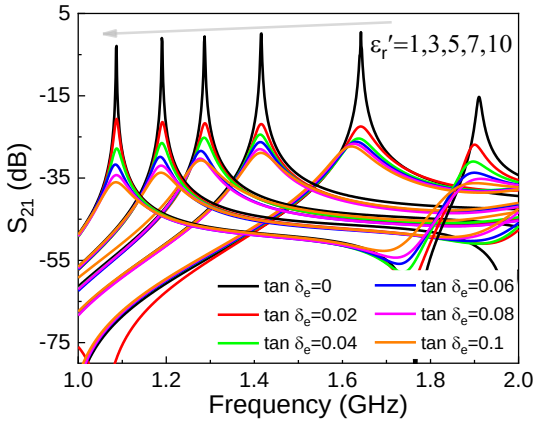

Fig. 5. Sensor responses for different values of (a) ε_r and (b) $\tan\delta_e$ when an MUT sample is placed on the sensing area.

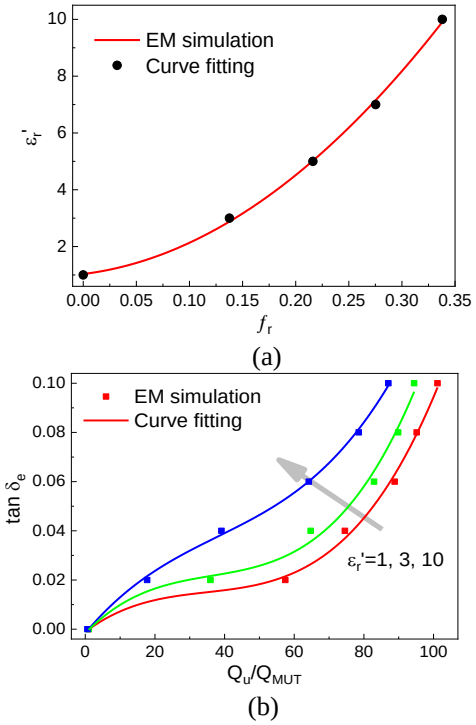

Fig. 6. Fitting curves for (a) ε_r' and (b) $\tan\delta_e$.

Owing to the effect of active loop, the proposed sensor possesses high quality factor, which is beneficial

to the extraction of resonant point as well as the design of peripheral circuit [13]. Moreover, as the loss tangent is usually retrieved by the variation in the quality factor, the sensor sensitivity in measuring the dielectric loss can be improved by employing the active loop [14]. With the help of curve fitting method, as shown in Fig. 6 (a), the function between relative permittivity ε_r' and resonant frequency shift Δf_r is given as:

$$\varepsilon_r' = 1.0033 + 8.607\Delta f_r + 17.044\Delta f_r^2, \quad (2)$$

where $\Delta f_r = (f_\mathrm{u} - f_\mathrm{MUT})/f_\mathrm{u}$, f_u denotes the resonant frequency of unloaded sensor, and f_MUT is the resonant frequency of the sensor with the MUT sample loaded.

When ε_r' is fixed, as shown in Fig. 5, the increase in the loss tangent $\tan\delta_e$ would result in a decrease in the quality factor. The loss tangent can be expressed as a function of inverse normalized quality factor, i.e., $Q_\mathrm{n} = Q_\mathrm{u}/Q_\mathrm{MUT}$, where Q_u and Q_MUT represent the quality factors of the sensors unloaded and loaded, respectively. As shown in Fig. 6 (b), the loss tangent $\tan\delta_e$ increases monotonically with the increase of Q_n and the fitting function is given as:

$$\tan\delta_e = \sum_{i=0}^{3} Q_\mathrm{n}^i \cdot \sum_{j=0}^{2} a_{ij}\,\varepsilon_r'^{\,j}. \quad (3)$$

The fitting coefficient a_{ij} ($i, j = 0$, 1, and 2) is listed in Table 2.

Table 2: Fitting coefficient a_{ij} for retrieving loss tangent

	$j=0$	$j=1$	$j=2$
$i=0$	−0.4796	−0.7459	−0.276
$i=1$	5.316×10^{-2}	-8.891×10^{-2}	3.736×10^{-2}
$i=2$	-3.745×10^{-2}	−0.2256	-4.297×10^{-3}
$i=3$	5.923×10^{-6}	-3.28×10^{-5}	4.509×10^{-5}

III. RESULTS AND DISCUSSION

To validate the ability of the proposed MCSRR-based sensor in characterizing dielectric materials, a prototype of the sensor was processed, as shown in Fig. 7 (a). The input and output ports of the sensor are mounted with 50 Ω SMA connectors for measuring the transmission data. The active loop is provided with 0.8 V bias voltage through the power supply. A number of dielectric materials are prepared and the transmission coefficients for testing these dielectric materials are recorded through the Keysight E5071C vector network analyzer (VNA).

Figure 7 (b) shows the measurement setup for the fabricated sensor. An 8.5 mm×5 mm×1 mm-size sample of the MUT is placed on the sensing area, and the transmission coefficients are recorded with the VNA. The measured sensor responses are shown in Fig. 8. For unloaded sensor, the resonant frequency is 1.546 GHz, and the quality factor is about 1288. The measured data are deviated from the simulated values, which may be due to the dielectric loss of resonator, the noises of the active loop, undesired signal at the frequency band, and the impact of the fluctuations in the environmental properties including temperature and humidity [15]. These deviations have little impact on the retrieval of the permittivity [16], and can be further suppressed by experimental calibration. For example, considering the deviations caused by manufacturing inaccuracies, the geometrical parameters of the fabricated sensor can be measured to correct the simulations [17]. Moreover, the measurement errors can be reduced by determining the fitting coefficients experimentally or adding error correction terms [18], [19]. Following the procedure described in [19], the fitting expressions are updated to increase the retrieval accuracy.

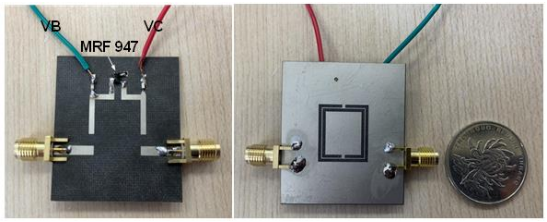

(a)

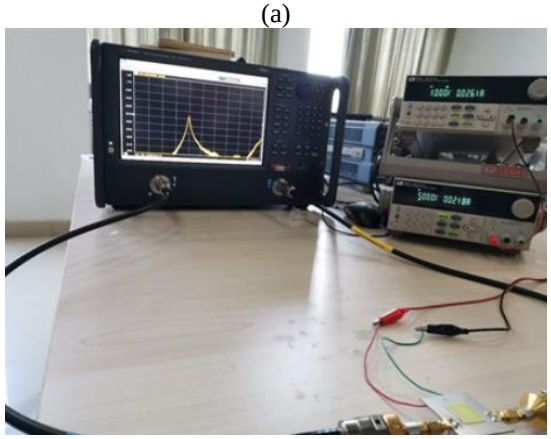

(b)

Fig. 7. (a) Photograph of the fabricated sensor and (b) experimental setup.

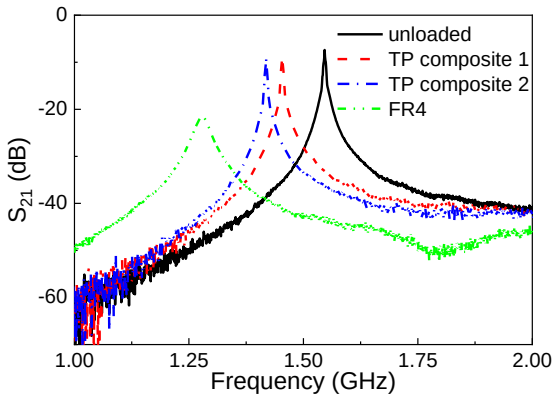

Fig. 8. Measured transmission coefficients.

Table 3: Comparison of the retrieved material parameters with reference values

	ε_r'		$\tan\delta_e$	
	Meas.	**Ref.**	**Meas.**	**Ref.**
TP composite 1	1.85	1.83	0	≤0.001
TP composite 2	2.23	2.2	0	≤0.001
FR4	4.51	4.4	0.018	0.02

Based on the measured data and fitting expressions, the complex permittivity of the MUT samples are calculated and compared with the reference values taken from manufacturer datasheets (see Table 3). The measured values are basically consistent with the reference values. Table 4 presents the comparison of the proposed sensor with previous designs. It is found that the proposed sensor has comparable performance but higher sensitivity and smaller electrical size than previous designs.

Table 4: Comparison of the proposed sensor with previous designs

	[11]	**[12]**	**Proposed**
Resonator	SRR	SRR	MCSRR
f_0 (GHz)	1.52	1.03/1.14	1.546
Q_0	1540	200	1288
Electrical size (λ_0^2)	0.132	0.121	0.052
S_{avg} ($\times 10^{-2}$)	0.17	0.36	4.67

III. CONCLUSION

In this paper, an MCSRR-based sensor was proposed for characterizing dielectric materials. The active feedback loop was employed to improve the quality factor, which is beneficial to the sensor resolution and the design of peripheral circuit. A prototype of the proposed sensor was fabricated and measured. It was demonstrated that the proposed sensor possesses high quality factor, small electrical size, and high sensor sensitivity, validating its potential for low-cost and precise characterization of dielectric materials.

ACKNOWLEDGMENT

This work was in part supported by NSFC under Grants 61874038, and the National Key R&D Program under Grant 2018YFE0120000.

REFERENCES

[1] S. O. Nelson and S. Trabelsi, "Dielectric spectroscopy measurements on fruit, meat, and grain," *Trans. ASABE*, vol. 51, no. 5, pp. 1829-1834, Oct. 2013.

[2] B. S. Cook, A. Shamim, and M. M. Tentzeris, "Passive low-cost inkjet-printed smart skin sensor for structural health monitoring," *IET Microw., Antennas Propag.*, vol. 6, no. 14, pp. 1536-1541, Nov. 2012.

[3] G. Gennarelli, S. Romeo, M. R. Scarfi, and F. Soldovieri, "A microwave resonant sensor for concentration measurements of liquid solutions," *IEEE Sensors J.*, vol. 13, no. 5, pp. 1857-1864, May 2013.

[4] J. Liu and P. B. Li, "Palladium decorated SWCNTs sensor for detecting methane at room temperature based on UWB-RFID," *Applied Computational Electromagnetics Society Journal*, vol. 31, no. 8, pp. 989-996, Aug. 2016.

[5] M. H. Zarifi and M. Daneshmand, "Liquid sensing in aquatic environment using high quality planar microwave resonator," *Sens. Actuators B, Chem.*, vol. 225, pp. 517-521, Mar. 2016.

[6] A. Ali, S. I. Jafri, A. Habib, Y. Amin, and H. Tenhunen, "RFID humidity sensor tag for low-cost applications," *Applied Computational Electromagnetics Society Journal*, vol. 32, no. 12, pp. 1083-1088, Dec. 2017.

[7] L. Su, J. Mata-Contreras, P. Vélez, and F. Martín, "Splitter/combiner microstrip sections loaded with pairs of complementary split ring resonators (CSRRs): Modeling and optimization for differential sensing applications," *IEEE Trans. Microw. Theory Tech.*, vol. 64, no. 12, pp. 4362-4370, Dec. 2016.

[8] A. Ebrahimi, J. Scott, and K. Ghorbani, ''Differential sensors using microstrip lines loaded with two split-ring resonators,'' *IEEE Sensors J.*, vol. 18, no. 14, pp. 5786-5793, July 2018.

[9] A. A. Abduljabar, D. J. Rowe, A. Porch, and D. A. Barrow, "Novel microwave microfluidic sensor using a microstrip split-ring resonator," *IEEE Trans. Microw. Theory Tech.*, vol. 62, no. 3, pp. 679-688, Mar. 2014.

[10] H.-Y. Gan, W.-S. Zhao, Q. Liu, D.-W. Wang, L. Dong, G. Wang, and W.-Y. Yin, "Differential microwave microfluidic sensor based on microstrip complementary split-ring resonator (MCSRR) structure" *IEEE Sensors J.*, vol. 20, no. 11, pp. 41985-41999, Feb. 2020.

[11] M. H. Zarifi, T. Thundat, and M. Daneshmand, "High resolution microwave microstrip resonator for sensing applications," *Sens. Actuators A, Phys.*, vol. 233, pp. 224-230, June 2015.

[12] M. Abdolrazzaghi and M. Daneshmand, "Dual active resonator for dispersion coefficient measurement of asphaltene nano-particles," *IEEE Sensors J.*, vol. 17, no. 22, pp. 7248-7256, Nov. 2017.

[13] B. Yu, X. Ding, H. Yu, Y. Ye, X. Liu, and Q. J. Gu, "Ring-resonator-based sub-THz dielectric sensor," *IEEE Microw. Wireless Compon. Lett.*, vol. 28, no. 11, pp. 969-971, Nov. 2018.

[14] W.-S. Zhao, H.-Y. Gan, Li. He, Q. Liu, D.-W. Wang, K. Xu, S. Chen, L. Dong, and G. Wang, "Microwave planar sensors for fully characterizing magneto-dielectric materials" *IEEE Access*, vol. 8,

pp. 41985-41999, Mar. 2020.
[15] H. Saghlatoon, R. Mirzavand, and P. Mousavi, "Fixed-frequency low-loss dielectric material sensing transmitter," *IEEE Trans. Ind. Electron.*, available online in early access.
[16] H.-Y. Gan, W.-S. Zhao, L. He, Y. Yu, K. Xu, F. Wen, L. Dong, and G. Wang, "A CSRR-loaded planar sensor for simultaneously measuring permittivity and permeability," *IEEE Microw. Wireless Compon. Lett.*, vol. 30, no. 2, pp. 219-221, Feb. 2020.
[17] S. Sun and W. Menzel, "Novel dual-mode Balun bandpass filters using single cross-slotted patch resonator," *IEEE Microw. Wireless Compon. Lett.*, vol. 21, no. 8, pp. 415-417, Aug. 2011.
[18] L.-C. Fan, W.-S. Zhao, D.-W. Wang, Q. Liu, S. Chen, and G. Wang, "An ultrahigh sensitivity microwave sensor for microfluidic applications," *IEEE Microw. Wireless Compon. Lett.*, vol. 30, no. 12, pp. 1201-1204, Dec. 2020.
[19] A. Kapoor, P. K. Varshney, and M. J. Akhtar, "Inter-digital capacitor loaded electric-LC resonator for dielectric characterization," *Microw. Opt. Technol. Lett.*, vol. 62, no. 9, pp. 2835-2840, Sep. 2020.

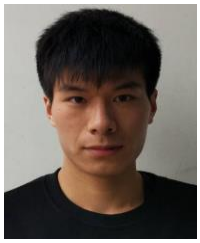

H.-Y. Gan is currently pursuing the M.E. degree with Hangzhou Dianzi University, Hangzhou, China. His research interest is focused on the design of microwave sensors.

W.-S. Zhao received the B.E. degree from Harbin Institute of Technology, Harbin, China, in 2008, and the Ph.D. degree from Zhejiang University, Hangzhou, China, in 2013.

As a part of his Ph.D. program, he visited the National University of Singapore (17 months) from 2010 to 2013. After graduation, he joined Hangzhou Dianzi University, Hangzhou, China, where he has been a Full Professor since January 2020. He as a Visiting Scholar with Georgia Institute of Technology from 2017 to 2018. He has two books, three book chapters, and more than 80 journal articles (including more than 40 IEEE papers). His current research interests include IC interconnect and packaging, electromagnetic devices, and electronic design automation.

Zhao is a senior member of IEEE and CIE, and serves as an associate editor for IEEE Access and an editor for Microelectronics Journal.

D.-W. Wang is currently an Associate Professor with Hangzhou Dianzi University, Hangzhou, China. His research interests include computational electromagnetics, multiphysics simulation, and signal integrity analysis.

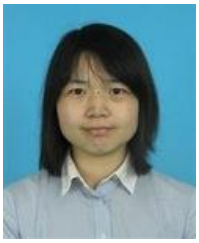

J. Wang is currently a faculty member with Hangzhou Dianzi University, Hangzhou, China. Her research interests include the design of tunnel transistors.

Q. Liu is currently a faculty member with Hangzhou Dianzi University, Hangzhou, China. Her research interests include the design and applications of microwave sensors.

G. Wang received the Ph.D. degree in Electrical Engineering from the University of Wisconsin-Milwaukee, WI, USA, in 1993, and the Ph.D. degree in Scientific Computing from Stanford University, Stanford, CA, USA, in 2001.

Wang is currently a Distinguished Professor with Hangzhou Dianzi University, Hangzhou, China. He has published more than 260 journal articles and held 48 patents. His current research interests include design, modeling, and simulation of IC and MEMS.